


# EO Africa // **ARIES**

**D19 – Final Report**  
**Version 1.0, November 2024**

**Contract No: 4000139191/22/I-DT**

submitted by

 <p>The logos of the three contributing organizations are stacked vertically. At the top is the VISTA logo, featuring a purple triangle with a white circle inside and the word 'Vista' in purple. Below it is the VITO logo, with a stylized bird icon and the text 'vito remote sensing'. At the bottom is the LIST logo, with the word 'LIST' in bold black letters and a colorful circular graphic to its right.</p>	<p>VISTA Remote Sensing in Geosciences GmbH (VISTA)</p> <p>Vlaamse Instelling voor Technologisch Onderzoek, Naamloze vennootschap (VITO)</p> <p>Luxemburg Institute of Science and Technology (LIST)</p>
---	--

## ESA STUDY CONTRACT REPORT

ESA Contract No 4000139191/22/I -DT	SUBJECT EO Africa // ARIES	CONTRACTOR VISTA Remote Sensing in Geosciences GmbH (VISTA)
* ESA CR( )No	* STAR CODE	Vol. 1
* ESA CR( )No		
<b>ABSTRACT:</b> <p>This document is the executive summary of the ARIES project activities and results.</p> <p>The copyright in this document is vested in VISTA GmbH. This document may only be reproduced in whole or in part, or stored in a retrieval system, or transmitted in any form, or by any means electronic, mechanical, photocopying or otherwise, either with the prior permission of VISTA GmbH or in accordance with the terms of ESA-ESRIN Contract No 4000139191/22/I-DT.</p> <p>Version 1.0</p> <p>Status: 26. Nov 2024</p>		
The work described in this report was done under ESA Contract. Responsibility for the contents resides in the author or organisation that prepared it.		
Names of authors: Silke Migdall (Vista), Jeroen Degerickx (Vito), Louis Snyders (Vito), Kanishka Mallick (List), Aolin Jia (List)		
<b>** NAME OF ESA STUDY MANAGER</b> Mr. Z. Szantoi DIV: EOP-SDR DIRECTORATE: Earth Observation Programmes	<b>** ESA BUDGET HEADING</b>	

## Authors of report

---

The present report was prepared by:

**Silke Migdall**

VISTA Geowissenschaftliche Fernerkundung GmbH  
(VISTA)

**Jeroen Degerickx, Louis Snyders**

Vlaamse Instelling voor Technologisch Onderzoek, Naamloze vennootschap  
(VITO)

**Kanishka Mallick, Aolin Jia**

Luxemburg Institute of Science and Technology  
(LIST)

## Content

---

<b>ESA STUDY CONTRACT REPORT .....</b>	<b>2</b>
<b>AUTHORS OF REPORT.....</b>	<b>3</b>
<b>CONTENT .....</b>	<b>4</b>
<b>FIGURES.....</b>	<b>5</b>
<b>LIST OF ACRONYMS .....</b>	<b>6</b>
<b>1 BACKGROUND &amp; INTRODUCTION.....</b>	<b>7</b>
<b>2 EXPERIMENTAL EO DATA PRODUCTS.....</b>	<b>7</b>
2.1 Thermal Data Products .....	7
2.1.1 Drought Index (LIST) .....	7
2.1.2 High-Resolution Crop Water Stress (VITO) .....	9
2.2 Hyperspectral Data Products (VISTA) .....	10
2.2.1 Leaf Area Index & Leaf Water Content.....	10
2.2.2 Canopy Water Content .....	11
<b>3 PRODUCT RESULTS, PROTOTYPING &amp; PLATFORM INTEGRATION.....</b>	<b>12</b>
3.1 Thermal Data Products .....	12
3.1.1 Drought Index (LIST) .....	12
3.1.2 High-Resolution Crop Water Stress (VITO) .....	14
3.1 Hyperspectral Data Products (VISTA) .....	17
3.1.1 Leaf Area Index .....	17
3.1.2 Canopy & Leaf Water Content.....	19
3.1 Integration in Food Security Explorer .....	22
<b>4 POLICY HIGHLIGHTS.....</b>	<b>24</b>
<b>5 RECOMMENDATIONS FOR CHIME AND LSTM .....</b>	<b>25</b>
5.1 LSTM.....	25
5.2 CHIME.....	26
<b>6 OUTREACH AND PROMOTION.....</b>	<b>27</b>
<b>7 CONCLUSION.....</b>	<b>28</b>
<b>8 REFERENCES .....</b>	<b>29</b>

## Figures

Figure 1 Drought indices captured the soil moisture anomalies (marked as blue).....	13
Figure 2 Land cover types surrounding the Mali site, and the spatial window size is 21 km. .	13
Figure 3 Monthly ESI maps at the Mali site (Lat: 16.6730 °, Long: -3.0448 °) in 2019 (a) July, (b) August, (c) September, and (d) October.....	14
Figure 4 Local drought mapping using (a) ECOSTRESS ESI, (2) MODIS STR, and (3) MODIS NDWI .....	14
Figure 5 Crop water stress indicator (LST-Ta in red) and NDVI (in green) time series for two specific locations at the AKTC test site in Zambia during the main agricultural season in 2024: (left) a large pivot, representing irrigated agricultural fields, (right) a typical example of non-irrigated agricultural field. Blue lines represent major precipitation events, based on CHIRPS rainfall data extracted from the FAO WaPOR data portal. The orange circle in both figures highlight key difference in terms of crop water stress between the two sites.....	15
Figure 6 Crop water stress indicator (LST-Ta in red) and NDVI (in green) time series for two specific locations at the ACF test sites in Mali during the main agricultural season in 2024: (left) an agricultural field which is known to have faced severe drought at the start of the season and has been partially destroyed by wildlife, (right) an agricultural field that has faced only mild consequences from drought. ....	16
Figure 7 True color RGB image of the surrounding landscape for the Mali test site. The red dot identifies the specific field for which the LST-Ta and NDVI time series are shown in Figure 9, right panel. ....	17
Figure 8 Leaf Area Index results calculated from PRISMA data acquired during the 2023 dry season at AKTC Zambia. ....	17
Figure 9 Leaf Area Index values calculated from PRISMA and EnMap data. Timeline at selected pixels within AKTC's irrigation pivots. Numbers correspond with locations indicated in Figure 8. ....	18
Figure 10 Leaf Area Index results calculated from PRISMA and EnMap data acquired during 2024 at the Mali test-site .....	19
Figure 11 Canopy Water Content results calculated from PRISMA data acquired during the 2023 dry season at AKTC Zambia.....	20
Figure 12 Leaf Water Content calculated from CWC and LAI derived from PRISMA data (31.07.2023).....	21
Figure 13 Canopy Water Content results calculated from PRISMA and EnMap data acquired in 2024 at the Mali test-site.....	21
Figure 14: Food Security Explorer – PERCEPTION view .....	22
Figure 15: Crop water stress indicator uploaded to the Food Security Explorer platform. ....	23
Figure 16: QGIS and EnMAP Toolbox on FS-X. Access to Plant Water Retrieval calculations as example.....	23
Figure 17: Retrieval of the Plant Water Content using the PWR Algorithm of the EnMAP Toolbox, visualisation as map and spectra of test pixel as illustrated.....	24
Figure 18: Example of striping in EnMAP data after plant water retrieval with EnMAP toolbox .....	26
Figure 19: Geometric offsets observed in PRISMA and EnMAP data at the AKTC test site. .	27

## List of Acronyms

---

ACF/AHH	Action contre la faim/Action Against Hunger
AGRHYMET	Centre régional de formation et d'application en agrométéorologie et hydrologie opérationnelle
AKTC	Zambian Agricultural Knowledge and Training Centre, LTD
ALIA	Average Leaf Angle
ASI	Agenzia Spaziale Italiana
CC	Correlation Coefficient
CWC	Canopy Water Content
DEM	Digital Elevation Model
DMS	Data Mining Sharpener
ECOSTRESS	ECOsysteM Spaceborne Thermal Radiometer Experiment on Space Station
EnMap	Environmental Mapping and Analysis Program
EO	Earth Observation
ERA	European Centre for Medium-Range Weather Forecasts atmospheric reanalysis
ESA	European Space Agency
ESI	Evaporative Stress Index
ET	Evapotranspiration
ET0	Reference Evapotranspiration
EU	European Union
GHG	Greenhouse gas
HR	High-Resolution
ISMN	International Soil Moisture Network
ISS	International Space Station
KBDI	Keetch-Byram Drought Index
LAI	Leaf Area Index
LiDAR	Light Detection and Ranging
LST	Land Surface Temperature
LUT	Look-up Table
LWC	Leaf Water Content
MODIS	Moderate Resolution Imaging Spectroradiometer
MW	Microwave
NASA	National Aeronautics and Space Administration
NDVI	Normalized Difference Vegetation Index
NDWI	Normalized Difference Water Index
NPV	Non-photosynthetic active vegetation
PRISMA	PRecursore IperSpettrale della Missione Applicativa
PWC	Plant Water Concentration
PWR	Plant Water Retrieval
RMS	Root-Mean-Square
RS	Remote Sensing
S2	Sentinel-2
S3	Sentinel-3
SDCI	Scaled Drought Condition Index
SLSTR	Sea and Land Surface Temperature Radiometer
SM	Soil Moisture
STD	Standard Deviation
STR	Shortwave Infrared Transformed Reflectance
SW	Split-Window
SWI	Soil Water Index
SWIR	Shortwave Infrared
TIR	Thermal Infrared

## 1 Background & Introduction

---

EO AFRICA (African Framework for Research Innovation, Communities and Applications) is a research and development initiative by ESA. It focuses on building African - European R&D partnerships and the facilitation of the sustainable adoption of Earth Observation and related space technology in Africa.

Within “ARIES” experimental EO analysis techniques are being developed and validated, addressing water management and food security in Africa.

To ensure the products developed within the project serve the needs of future users the techniques are being developed closely together with African Early Adopters. These five organizations are covering east (AfriGeo, EO research group within the Regional Centre for Mapping of Resources for Development in Kenya & the Regional Centre for Mapping of Resources for Development in Kenya itself), west (AGRHMET Regional Centre and AAH Action Against Hunger in Niger) and southern (Zambian Agricultural Knowledge and Training Centre LTD in Zambia) Africa. Thereby the developed algorithms and approaches can be validated, tested and evaluated in different geographic regions with different climatic conditions and agricultural practices.

## 2 Experimental EO Data Products

---

### 2.1 Thermal Data Products

#### 2.1.1 Drought Index (LIST)

Drought is characterized by a prolonged deficiency in water supply, affecting various aspects such as the atmosphere, soil, streamflow, groundwater, and economic activities (AghaKouchak et al., 2015). It poses substantial challenges to socioeconomic systems, leading to issues like food security, water resource inequality, and environmental degradation, including desertification and debris flow. Africa emerges as a focal point for drought-induced global change, with frequent hazards adversely affecting biodiversity and natural resource sustainability (Hadebe et al., 2017). The increasing frequency of drought exacerbates these challenges, resulting in tropical wildfires, heatwaves, and affecting approximately 20% of the population with hunger (Otekunrin et al., 2020). Urgent efforts are needed for effective drought monitoring in Africa. Diverse drought indices, reliant on meteorological variables and remote sensing (RS) data, have been developed.

Regional applicability of meteorological drought indices faces challenges due to the limited coverage of ground-based monitoring stations. In comparison, satellite RS offers a promising alternative by leveraging indirect indicators such as green vegetation dynamics and land surface temperature (LST) variations. Nevertheless, RS-based indices encounter limitations such as infrequent temporal sampling and cloud cover (Jia et al., 2022). Furthermore, they often lack clear physical interpretations essential for effective water resource management and policy development. Soil moisture RS products are available on a daily basis, whereas they are constrained by coarse spatial resolutions ( $> 9$  km), restricting their effectiveness for localized irrigation planning. Additionally, the validation of existing drought indices, remains insufficient across diverse landscapes and climatic conditions in Africa. Addressing these gaps is crucial for enhancing the reliability and applicability of drought monitoring systems across the region.

Therefore, developing drought indices that incorporate thermal and optical data from advanced remote sensing (RS) sensors will significantly improve our ability to monitor agricultural drought at the local level. The ECOSystem Spaceborne Thermal Radiometer Experiment on Space Station (ECOSTRESS) was deployed aboard the International Space Station (ISS) on June 29, 2018 (Fisher et al., 2020). It Serves as a pioneering mission for forthcoming Thermal Infrared (TIR) endeavors, capturing thermal imagery across five bands spanning 8 to 12.5  $\mu\text{m}$ . With its advanced capabilities, it achieves high spatio-temporal resolution, obtaining TIR data at various times throughout the day. Through resampling at the nadir, ECOSTRESS achieves a pixel size of approximately  $70 \times 70$  m, facilitating the retrieval of evapotranspiration (ET) data at fine spatial scales, including small ecosystem patches and individual agricultural fields. The revisit time averages between 1 to 5 days, significantly surpassing previous high resolution thermal missions (e.g., Landsat). In regions with high latitude where the ISS orbital path varies, observation frequency can increase, allowing multiple observations within a single day. This frequent observation capability is particularly advantageous for assessing agricultural heat and water stress (Jia et al., 2024). Therefore, within this project, thermal drought indices will be utilized using ECOSTRESS data alongside other high-resolution optical data across Africa.

Evaporative Stress Index (ESI), calculated based on ECOSystem Spaceborne Thermal Radiometer Experiment on Space Station (ECOSTRESS) evapotranspiration product, is proposed as the primary thermal drought index in the project. In addition, several meteorological and agricultural drought indices are employed for the evaluation and inter-comparison.



The Keetch-Byram Drought Index (KBDI), calculated using maximum daily temperature and total daily precipitation from the fifth-generation European Centre for Medium-Range Weather Forecasts atmospheric reanalysis v5 (ERA5), serves as a meteorological drought index. Shortwave Infrared Transformed Reflectance (STR), derived from Moderate Resolution Imaging Spectroradiometer (MODIS) shortwave infrared reflectance sensitive to water content, is used as a representative RS-based index. Additionally, a hybrid Scaled Drought Condition Index (SDCI) is involved, calculated using normalized MODIS LST, Normalized Difference Vegetation Index (NDVI), and precipitation from ERA5. To better validate the drought indices, in-situ SM from 36 sites within the International Soil Moisture Network (ISMN) in Africa serves as the ground truth for agricultural drought signals. The drought indices were implemented at 8-day and monthly scales.

### 2.1.2 High-Resolution Crop Water Stress (VITO)

The most straightforward way to derive crop water stress information from thermal Earth Observation measurements, is to compute the difference between ambient air temperature ( $T_{air}$ ) and the land surface temperature (LST), as indicated by e.g. Idso et al. (1977). The general concept here is that crops having insufficient access to water resources tend to close their stomata to limit excessive water loss through transpiration. As a result, the leaf surface of the crop heats up compared to the surrounding air. Hence, strongly positive values of  $LST - T_{air}$  indicate water stress in crops. Currently, the main limitation to offer such a product in an operational setting is the lack of high spatial and temporal resolution thermal satellite data. While waiting for future thermal satellite missions to bridge this gap, several data sharpening techniques have been proposed to generate high-resolution LST data based on lower resolution alternative data sources. One such popular approach is the Sen-ET algorithm, which generates 20 m daily LST data based on a data fusion approach between 1 km thermal data from Sentinel-3 (S3) and 20 m optical data from Sentinel-2 (S2).

Three main problems can be identified regarding this sharpened 20 m LST product from Sentinel-3:

1. Generally, the operational Sentinel-3 SLSTR split-window (SW) algorithm systematically overestimates LST, due to wrongly assigned land covers and corresponding SW coefficients (Pérez-Planells et al., 2021; Sanchez et al., 2024).
2. Although the thermal sharpening procedure ensures conservation of surface energy between the low- and high-resolution products, sharpened high-resolution LST products (especially when sharpening ratios are high as is the case for S3), are known to suffer from a loss of LST dynamic contrast compared to an LST product originally captured at high resolution. Bellvert et al. (2020) for

instance concluded that extremes in LST were not properly captured in S3 sharpened LST imagery, making it less suited for precision agriculture applications as compared to high-resolution LST imagery. This is especially true for highly heterogeneous scenes such as orchards or complex agricultural landscapes in a smallholder farming context.

3. Directional effects caused by sun-sensor geometry variations between subsequent LST observations typically can result in LST differences of more than 10 K (Lagouarde & Irvine, 2008), causing important inconsistencies in LST time series.

Given these remaining issues, we suggest adding a two-stage LST correction procedure to produce higher quality high-resolution LST measurements. The first stage involves cross-calibrating the thermally sharpened LST with ECOSTRESS LST to compensate for the known quality issues with S3 data itself and the sharpening procedure. The second stage entails the quantification of directional effects by comparing simultaneous acquired cross-calibrated thermally sharpened S3 images and ECOSTRESS with different viewing geometry. This allows to remove the directional effects in the high-resolution S3 LST.

## **2.2 Hyperspectral Data Products (VISTA)**

### **2.2.1 Leaf Area Index & Leaf Water Content**

Leaf Area Index (LAI) is defined as the amount of leaf area ( $\text{m}^2$ ) in a canopy per unit ground area ( $\text{m}^2$ ) (Watson 1947). It is a critical variable for applications ranging from climate science to food security and agriculture as it is one of the main driving forces of net primary production, water and nutrient use, and carbon balance. As such, it is an essential variable in describing and quantifying processes such as photosynthesis, respiration, precipitation interception and carbon build-up as well as an indicator for plant health and development (Bréda 2008, GCOS 2011, Asner et al. 1998, Ballaré et al. 2012)

The Leaf Water Content (LWC) is defined as the content of water per leaf area ( $\text{g}/\text{cm}^2$ ). Multiplied by the leaf area, the water content of the plant can be calculated. The plant water is an important indicator of the current status of the plant concerning its water demand and the possible need for irrigation (Quemada et al. 2021).

LAI can be determined in the field through a variety of direct and indirect methods (Fang et al. 2019). Moreover, retrieving LAI from remote sensing data has been extensively studied over the last few decades (Goel 1989, Baret 2015, J. M. Chen 2018, Houborg et al. 2007, Verrelst et al. 2015, Zheng & Moskal 2009). Retrieval methods have been developed for a wide range of data captured mainly by passive multispectral,

microwave and LiDAR sensors (Fang et al. 2019). More recently the developed methods, which can be categorized into empirical transfer functions and model inversion methods, are being expanded to upcoming hyperspectral sensors (Berger et al. 2018). The latter make use of a radiative transfer model, with the aim of establishing a relationship between fundamental canopy, soil and leaf properties, such as LAI, and the scene reflectance, given a specific sun-surface-sensor geometry (Goel & Thompson, 2000; S. Liang, 2004). PROSAIL (Berger et al., 2018, Jacquemoud et al. 2009), which combines the PROSPECT leaf optical properties model (Jacquemoud & Baret, 1990) and the SAIL canopy bidirectional reflectance model (Verhoef, 1984) has become one of the most popular radiative transfer tools. It is generally user friendly, robust and has been consistently validated in laboratory, field and space experiments over an extended period, during which it has also been under continual development (Jacquemoud et al. 2009, Verhoef & Bach 2003, Weiss et al. 2001, Kuusk 1991, Verhoef et al. 2007, Verhoef & Bach 2007, Jacquemoud et al. 1996, Fourty et al. 1996, Le Maire et al. 2004, Feret et al. 2008, Feret et al. 2017, Feret et al. 2021). One way to apply the model is to generate a set of modelled reflectance spectra based on a set of properly configured input variables and stored in a look-up table (LUT). The subsequent inversion process determines the set of canopy biophysical variables, aiming for the best match between the calculated and the remotely sensed reflectance (D. Huang et al. 2008, Verrelst et al. 2014).

### 2.2.2 Canopy Water Content

Canopy water content (CWC) is a vital parameter to monitor the plant status and support a balanced water supply and irrigation. Water stored in agricultural plants is linked to biochemical factors such as vegetation transpiration (Running et al., 1991) and net primary production. Especially for agricultural management in arid regions, accurate retrieval of the water content and vegetation traits might be crucial for mitigating water stress due to climate-related droughts and heat-waves (Tagliabue et al., 2022).

For canopy water retrieval from hyperspectral, it is possible to use the specific H<sub>2</sub>O water absorption features contained in the detailed reflectance spectra. This is a difference to multi-spectral data, which significantly broader and significantly less bands and thus can only estimated the water content via broad changes in the spectrum (e.g. lower value in the short-wave infrared). Hence, where multi-spectral indices only allow for a qualitative derivation of the canopy water content, the hyperspectral absorption features allow for a quantitative derivation of the canopy water content.

The Plant Water Retrieval (PWR) extracts quantitative water content information in [g cm<sup>-2</sup>] or [cm] from hyperspectral images. It is implemented in the EnMAP-Box (Wocher et al. 2018). It applies the Beer-Lambert law to inversely determine the optical

thickness  $d$  of the water layer responsible for the water absorption feature at 970 nm using water absorption coefficients for pure liquid water.

### 3 Product Results, Prototyping & Platform Integration

---

#### 3.1 Thermal Data Products

##### 3.1.1 Drought Index (LIST)

A correlation coefficient (cc) analysis was conducted across all ground sites to examine the relationship between ISMN SM and various drought indices. The corresponding statistical results are presented in Table 1. The median cc serves as a measure of overall performance, while the standard deviation (STD) is provided to account for variations in performance across different sites at 8-day and monthly scales.

**Table 1 Median value at different sites and overall standard deviation (STD) statistics of Correlation coefficient (cc) between in-situ SM and drought indices.**

Index	8-day		monthly	
	cc	STD	cc	STD
SMAP	0.85	0.07	0.88	0.11
SWI	0.88	0.12	0.91	0.21
KBDI	-0.47	0.17	-0.55	0.24
SDCI	0.40	0.15	0.44	0.24
STR	0.60	0.21	0.61	0.25
ESI	0.49	0.16	0.53	0.19

Table 1 reveals that SMAP and SWI exhibit the highest median correlation coefficients (cc) close to 0.9, with SMAP displaying significantly lower STD, signifying a more consistent performance across diverse conditions compared to ESA SWI. Notably, all meteorological and remote sensing drought indices fall short in capturing the temporal variability of SM when compared to MW SM products. The cc values hover around 0.5, with a corresponding STD of 0.17. Notably, STR outperforms others, and post time upscaling, KBDI and STR demonstrate similar performance. ESI, with considerably fewer data points, exhibits a performance gap possibly attributed to data scarcity.

After removing the seasonality to detect the anomalous SM signals, the temporal variability of different drought index and soil moisture anomalies are shown in Figure 1.

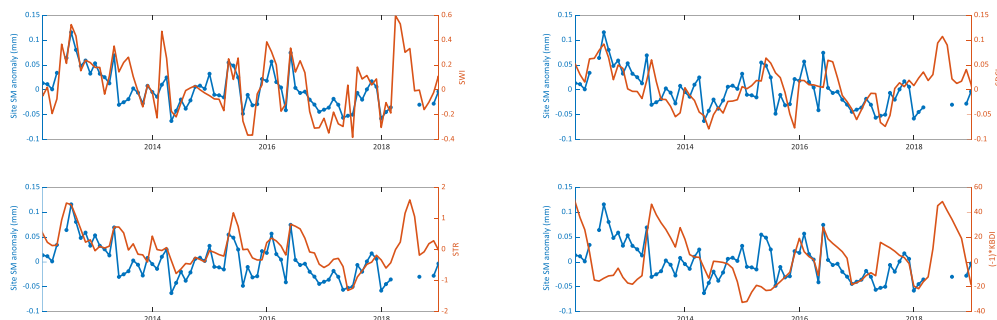


**Figure 1 Drought indices captured the soil moisture anomalies (marked as blue)**

In comparison, ECOSTRESS ESI shows the ability to map the drought stress at local scales. The Mali site (Lat: 16.6730 °, Long: -3.0448 °) was selected for local mapping analysis. The land cover type map (Figure 2) indicates the high heterogeneity around the site. The land cover type data is from Copernicus Global Land Cover Layers (CGLS-LC100) with 100m spatial resolution.

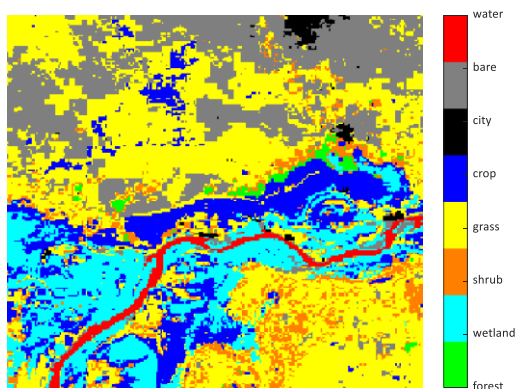


**Figure 2 Land cover types surrounding the Mali site, and the spatial window size is 21 km.**

The monthly ESI is subsequently mapped, revealing distinct temporal variations (Figure 3). Spatial patterns align closely with land cover characteristics, notably indicating lower drought stress in wetlands during October in comparison to grassland and barren land (Fig. 3d). Figure 3 underscores the potential utility of ESI for localized drought stress monitoring.

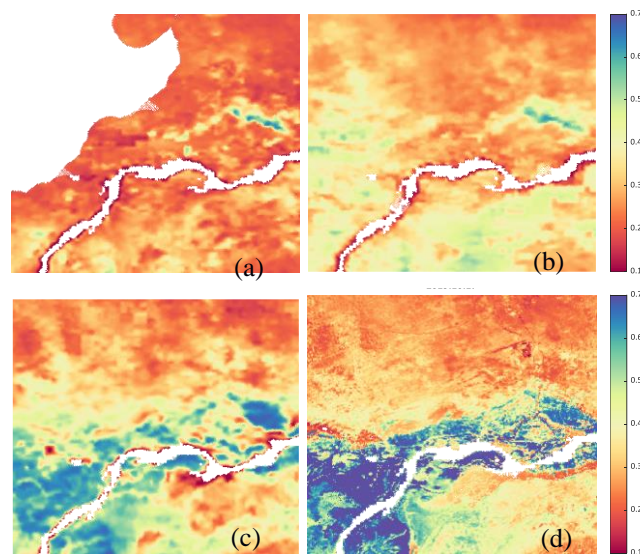


**Figure 3** Monthly ESI maps at the Mali site (Lat: 16.6730 °, Long: -3.0448 °) in 2019 (a) July, (b) August, (c) September, and (d) October.

Even when averaging ESI images within a month, the ESI for July (Figure 3) exhibits a distinct data gap. This underscores the imperative to reconstruct the LST data, prior to its application to fully leverage drought indices derived from high-resolution remote sensing. The image comparison in Figure 4 with other indices demonstrates that high-resolution thermal data shows its better performance in mapping drought at local scales. In addition, due to the short span and limited sampling frequency of ECOSTRES data, detrending cannot be done, thus the seasonal cycle may also impact the results.

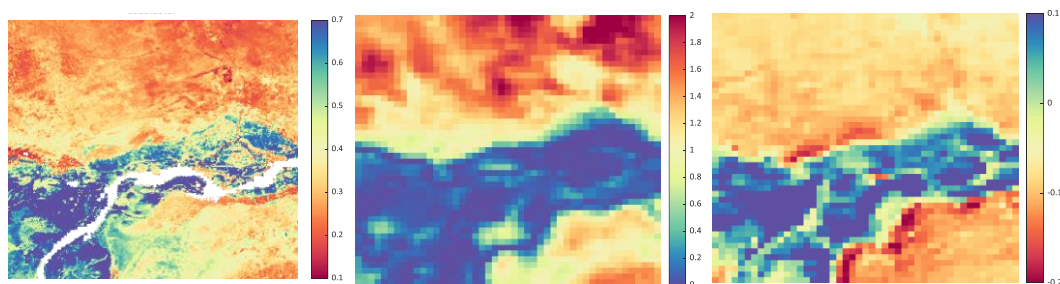


**Figure 4** Local drought mapping using (a) ECOSTRESS ESI, (2) MODIS STR, and (3) MODIS NDWI

### 3.1.2 High-Resolution Crop Water Stress (VITO)

The crop water stress indicator has been computed over the test sites located in Zambia (AKTC) and Mali (ACF). Some results for Zambia are summarized in Figure 5.



Three important observations can be made based on this figure, confirming the LST-Ta indicator is working as intended and is indeed sensitive to crop water stress:

- 1) The LST-Ta indicator is highly sensitive to land cover, showing high values when the field is bare and low values when covered by a crop. This highlights the need to always account for land cover when interpreting this indicator (hence the inclusion of NDVI in the figure).
- 2) As can be seen in the left panel of the figure, LST-Ta indicator drops significantly following a major precipitation event, after which it slowly increases again. This is completely expected behaviour in a hot climate where water stress kicks in relatively quickly following a precipitation event.
- 3) During the growing season, the LST-Ta indicator shows distinctive peaks on the rainfed site, which are not present on the irrigated plot, indicating more crop water stress in the non-irrigated site, which is completely in line with expectations. This shows indeed that this specific indicator is sensitive to capturing the impact of irrigation practices on crop water stress, and potentially, productivity.

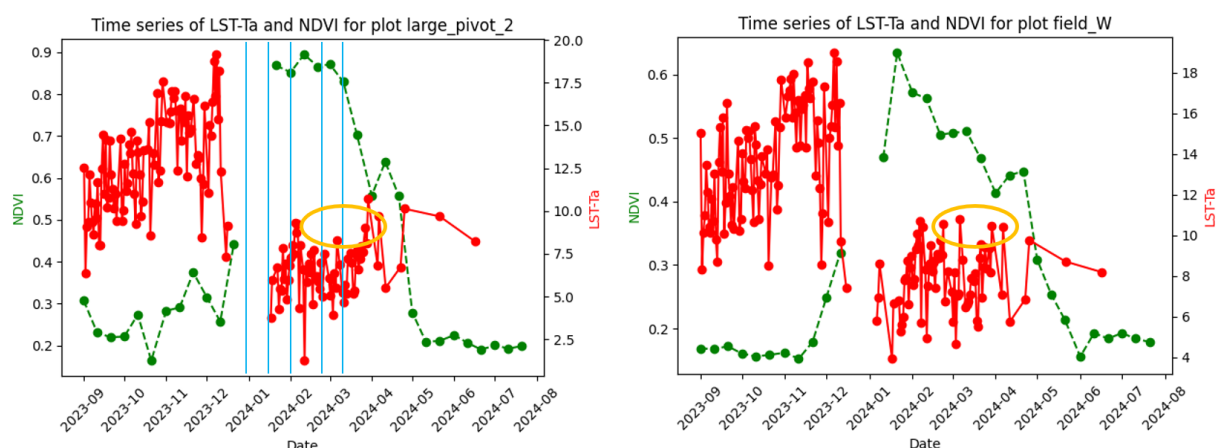


**Figure 5** Crop water stress indicator (LST-Ta in red) and NDVI (in green) time series for two specific locations at the AKTC test site in Zambia during the main agricultural season in 2024: (left) a large pivot, representing irrigated agricultural fields, (right) a typical example of non-irrigated agricultural field. Blue lines represent major precipitation events, based on CHIRPS rainfall data extracted from the FAO WaPOR data portal. The orange circle in both figures highlight key difference in terms of crop water stress between the two sites.

When applying the crop water stress indicator to the Mali test sites, the limitations of the approach become apparent. As shown in Figure 6, left panel, for some fields the crop water stress indicator does make sense, showing relatively low values during the growing season, high values during periods of bare soil and a peak in crop water stress at the start of the growing season, matching the reported severity of drought for that particular field. On the other hand, the right panel of the same figure shows an example

of a field where the derived crop water stress indicator shows no or limited correlation with land cover (as represented by the NDVI time series). This is a clear case where the results of the LST sharpening procedure cannot be trusted and final results should be interpreted with great care. This can be explained by considering the broader context of the specific agricultural field (Figure 7). Most of the area consists of desert, with only limited agricultural activities. In order for the LST sharpening approach to work, one needs a good amount of relatively homogeneous 1km x 1km pixels, especially over agricultural areas. On the Mali test site, this is clearly not the case, leading to unstable and unreliable high-resolution LST estimates. As said, this clearly implies the method cannot readily be applied anywhere. Future, higher spatial resolution thermal sensors will play a key role in alleviating this current limitation.

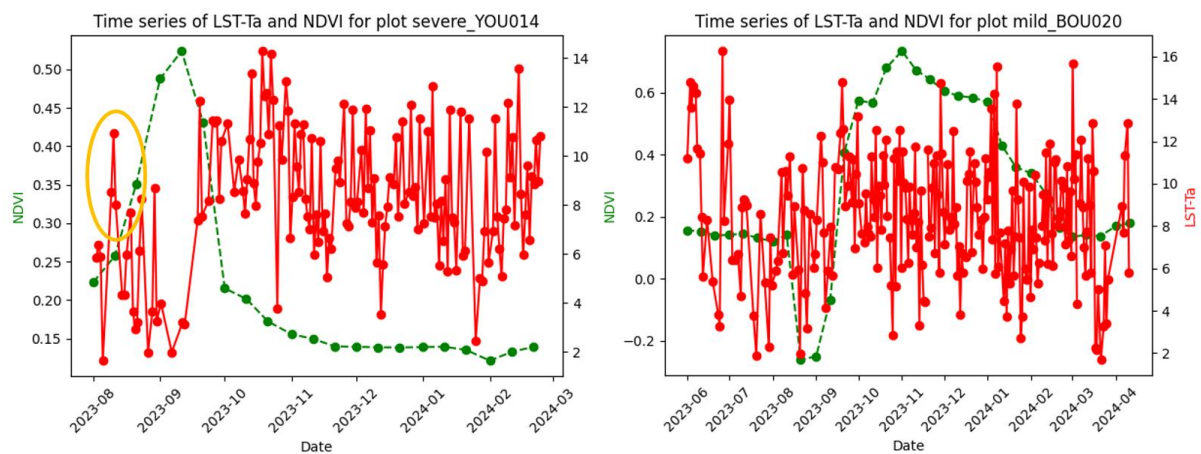


**Figure 6** Crop water stress indicator (LST-Ta in red) and NDVI (in green) time series for two specific locations at the ACF test sites in Mali during the main agricultural season in 2024: (left) an agricultural field which is known to have faced severe drought at the start of the season and has been partially destroyed by wildlife, (right) an agricultural field that has faced only mild consequences from drought.





**Figure 7** True color RGB image of the surrounding landscape for the Mali test site. The red dot identifies the specific field for which the LST-Ta and NDVI time series are shown in Figure 9, right panel.

The workflows that generate the crop water stress indicator have been published in an open-source GitHub repository. These workflows in addition contain the necessary tools to upload the generated products to the Food Security Explorer platform.

### 3.1 Hyperspectral Data Products (VISTA)

#### 3.1.1 Leaf Area Index

LAI values were determined across the test site via model inversion of the PROSAIL model available within the EnMap toolbox. This was done for all available EnMap and PRISMA data takes (selected results in Figure 8) and a timeline of LAI results was created for several pixels within the irrigation pivots where wheat was being cultivated during the 2023 dry season (Figure 9). The area surrounding point 4 was not planted in 2023 (see Figure 8 Leaf Area Index results calculated from PRISMA data acquired during the 2023 dry season at AKTC Zambia.).

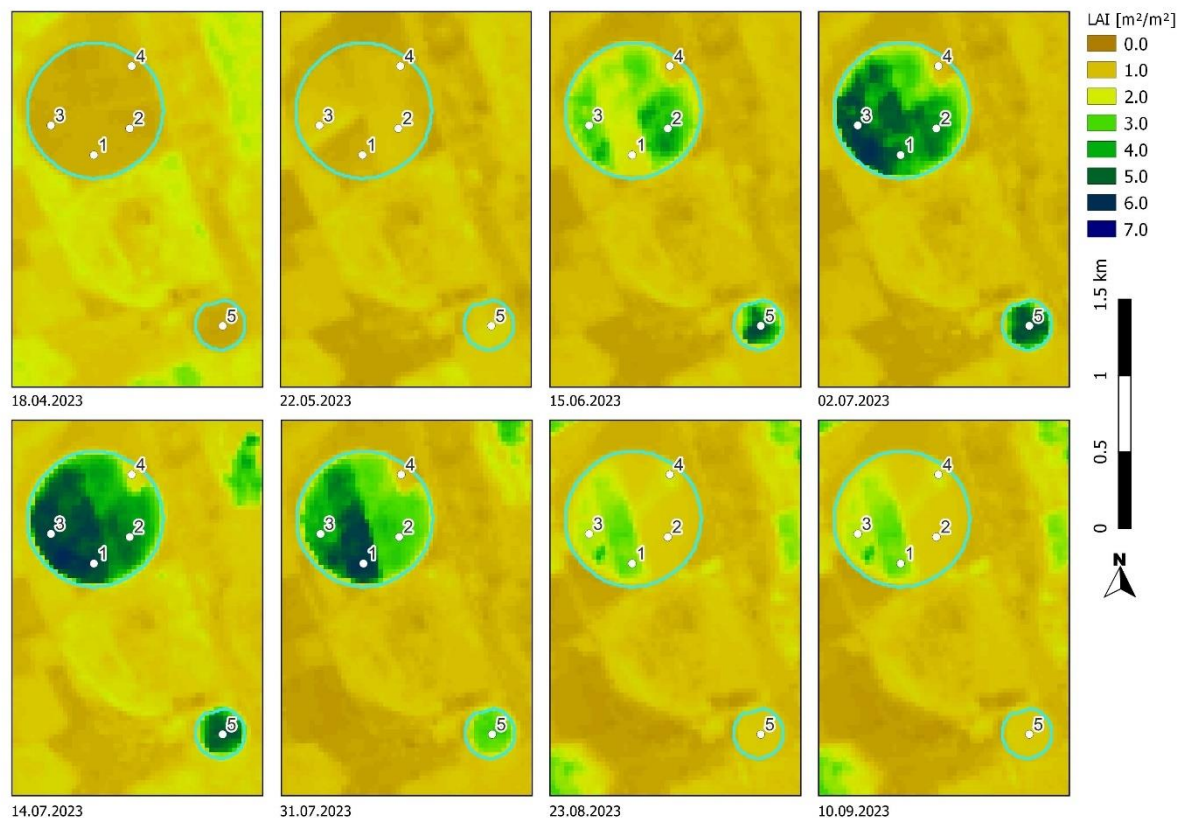


**Figure 8** Leaf Area Index results calculated from PRISMA data acquired during the 2023 dry season at AKTC Zambia.

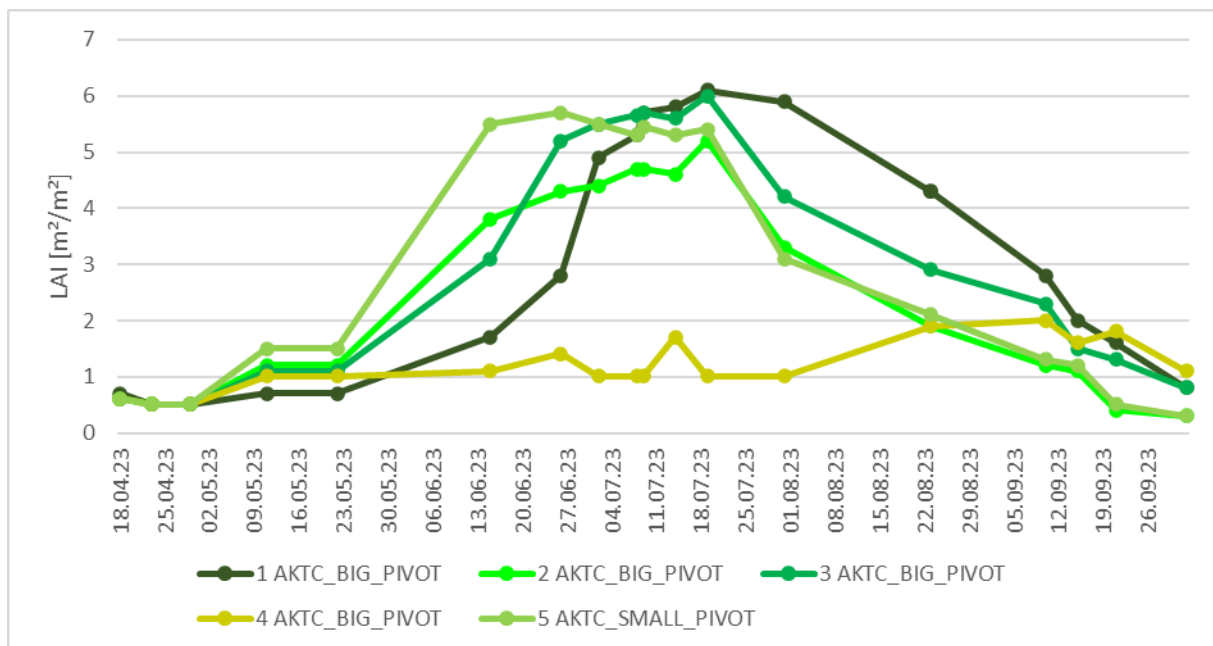


**Figure 9 Leaf Area Index values calculated from PRISMA and EnMap data. Timeline at selected pixels within AKTC's irrigation pivots. Numbers correspond with locations indicated in Figure 8.**

The time-series was also calculated for the Mali test-site and is shown in the following figure. Difference in LAI development are visible also in this drier area. Overall, the LAI values are smaller than in the irrigated fields in Zambia.

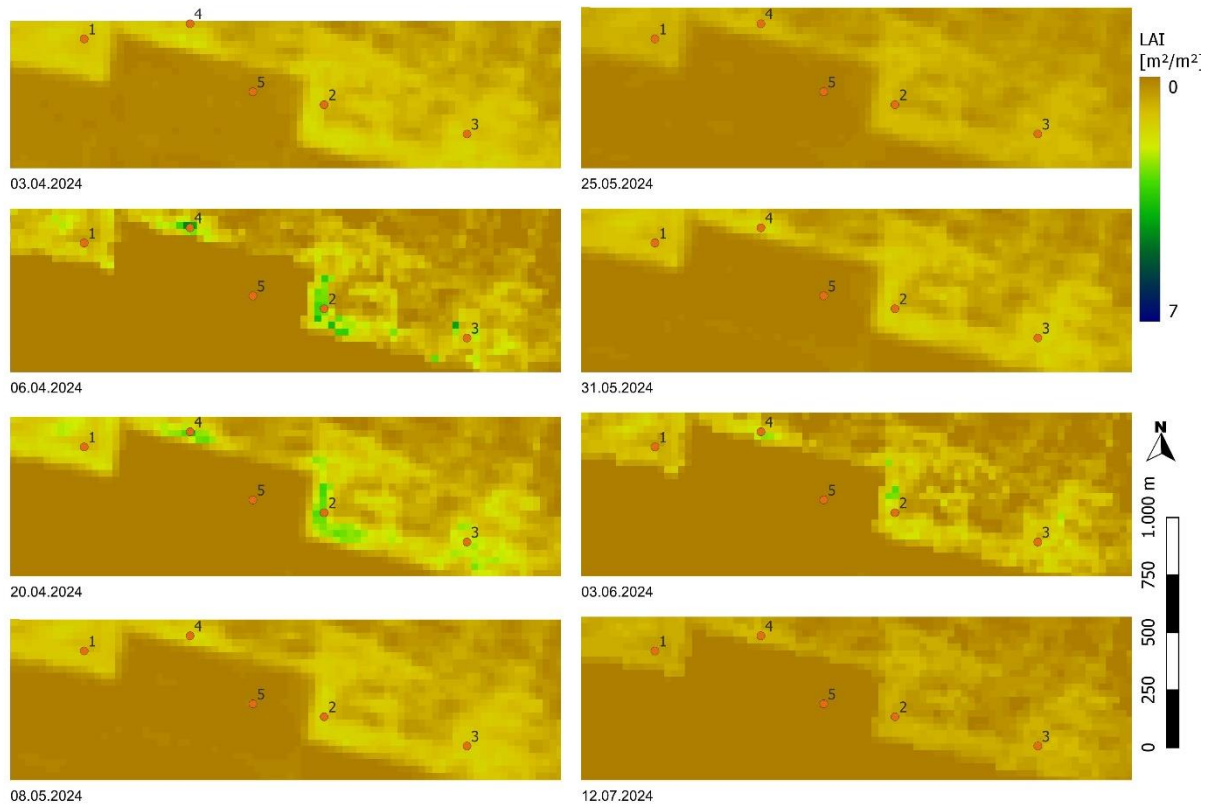
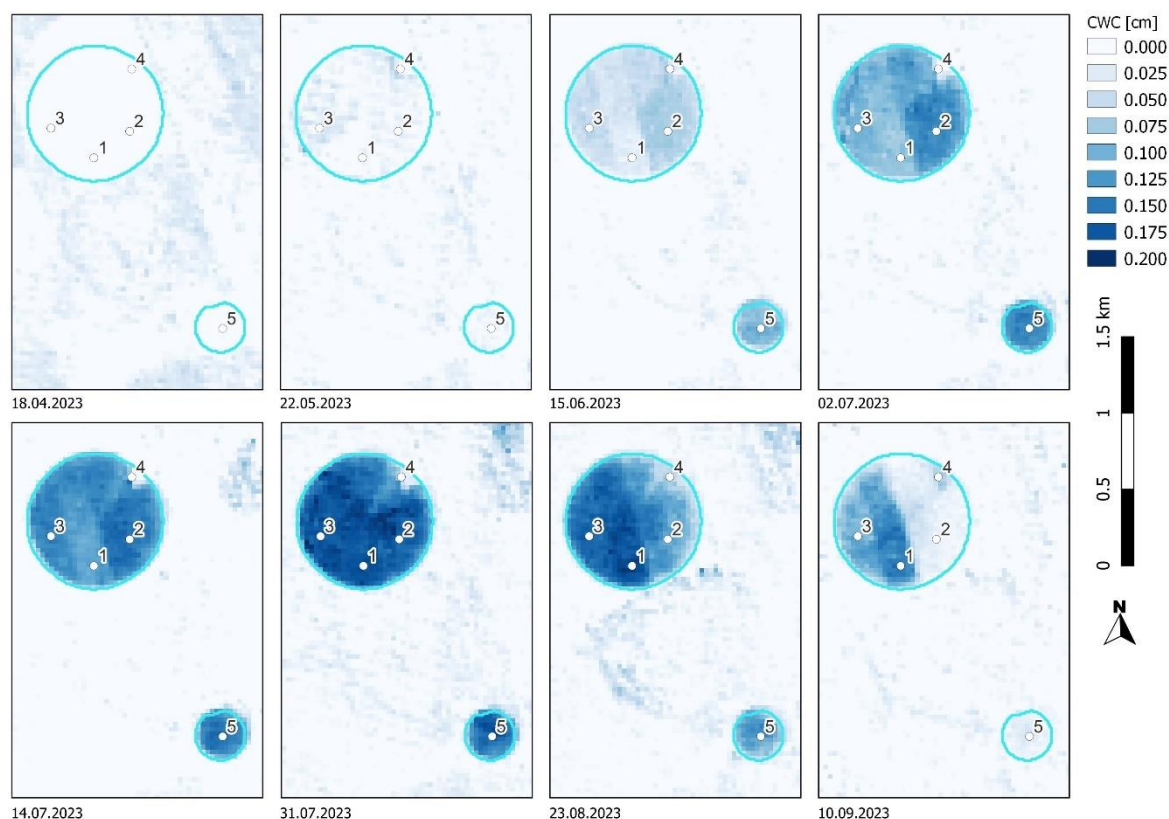


Figure 10 Leaf Area Index results calculated from PRISMA and EnMap data acquired during 2024 at the Mali test-site

### 3.1.2 Canopy & Leaf Water Content

Canopy Water Content was calculated using the Plant Water Retrieval (PWR) Tool available within the EnMap toolbox (Figure 11).



**Figure 11 Canopy Water Content results calculated from PRISMA data acquired during the 2023 dry season at AKTC Zambia.**

The method was developed by Wocher et al. 2018. Included in its implementation within the EnMap toolbox is a calibration factor which has been validated through performance assessment. The PWR tool has proven its ability to accurately predict plant water conditions as found in samples taken at winter wheat and corn test sites in Bavaria. The transferability of the method was also shown (Wocher et al. 2018). While validation with in-situ data still helps to prove the robustness of results, it is not strictly necessary. The method was chosen with regards to the unavailability of quantitative plant water data at the AKTC test site.

Leaf Water Content was then derived by combining LAI and CWC results (Figure 12 Leaf Water Content calculated from CWC and LAI derived from PRISMA data (31.07.2023)). As the intermediate products have already been validated or do not need validation, no separate validation has been conducted for LWC.

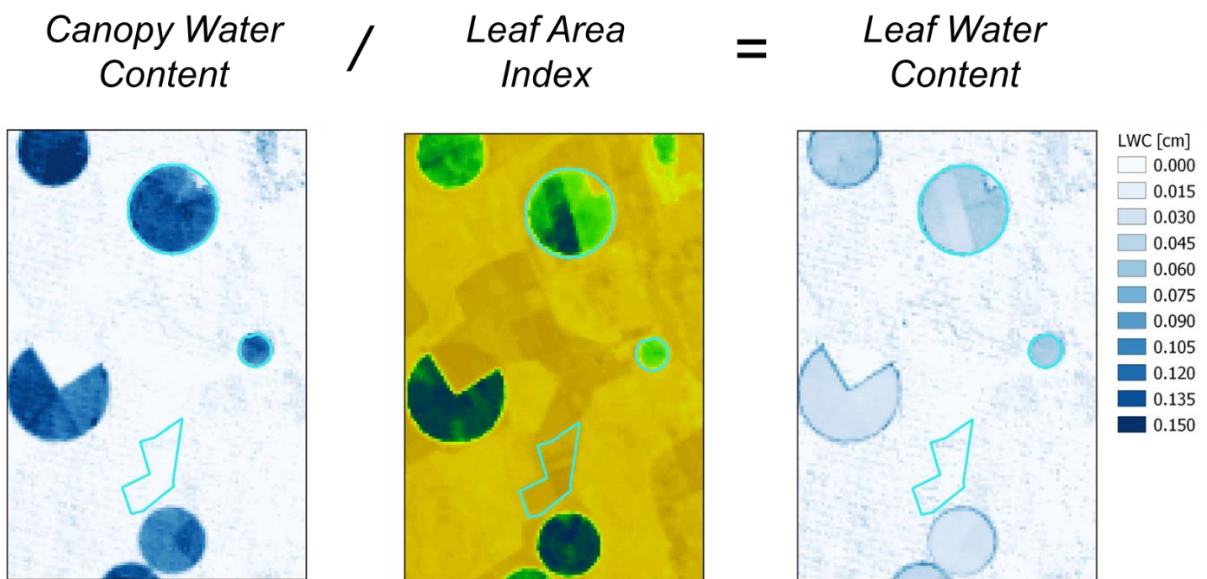


Figure 12 Leaf Water Content calculated from CWC and LAI derived from PRISMA data (31.07.2023)

The time-series was also calculated for the Mali test-site and is shown in the following figure.

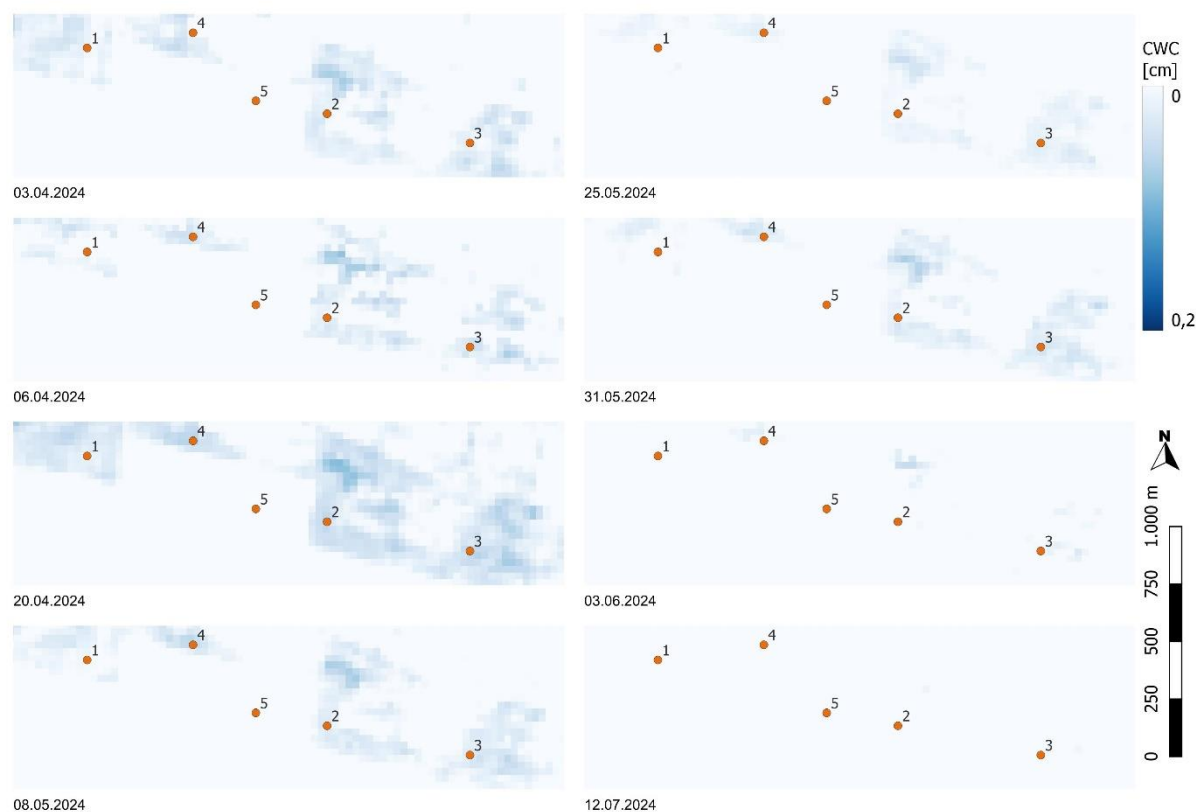


Figure 13 Canopy Water Content results calculated from PRISMA and EnMap data acquired in 2024 at the Mali test-site



### 3.1 Integration in Food Security Explorer

After development of the algorithms, the next aim of ARIES was to deploy a prototype with the active involvement of African end-users, so that they can test the innovative EO solutions. Additionally, the prototype was used to trigger interest by a wider community of potential stakeholders, as it is integrated into the Food Security Explorer (<https://foodsecurity-explorer.com>) (formerly Food Security-TEP) and thus is publicly available. For the sponsoring of platform services for the data processing and prototype hosting needed by the project, a Network of Resources (NoR) sponsorship (<https://portfolio.nor-discover.org/>) was requested and granted by ESA. The Food Security Explorer hosts many datasets relevant for this project, including the full range of the Copernicus acquisitions via connection to the CDSE as well as directly hosting the ECOSTRESS dataset, which was of course very relevant for this project.

The test prototype implementation followed Agile Development methods and engineering best practices. This allowed to rapidly move from the initial algorithm/s and processor assessment, towards the test prototype, while maintaining iterative interactions with the Early Adopters and frequent development cycles.

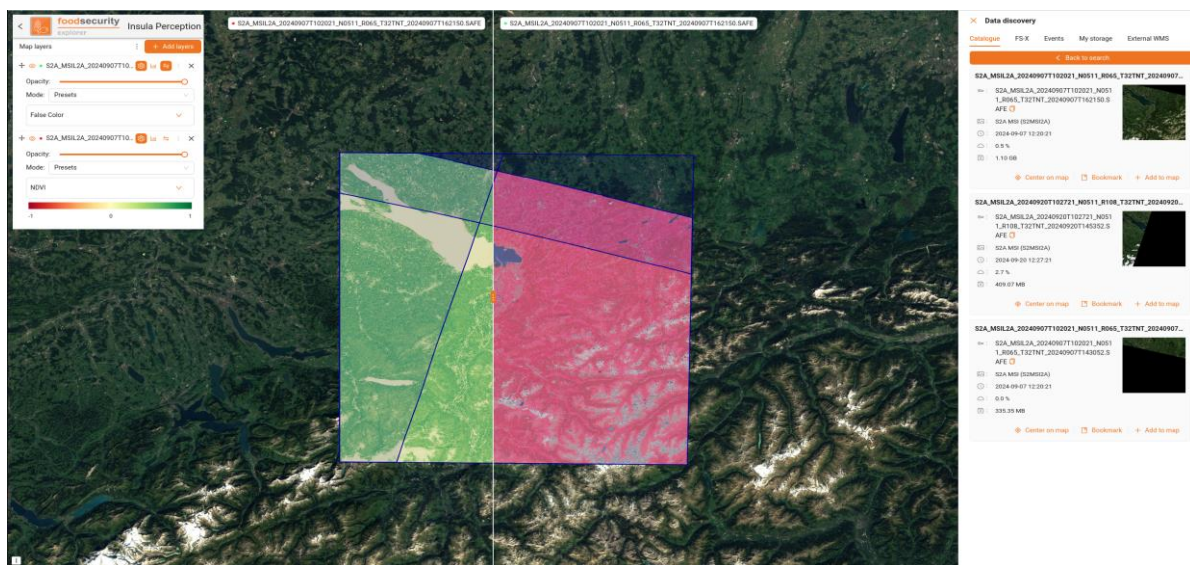


Figure 14: Food Security Explorer – PERCEPTION view

For data discovery and analytics, a PERCEPTION (previously called DAMA - Data Analytics and Management) component is integrated. Also, an INTELLECT (previously called SIR - Service interface Runner) component is available for processing in different modes. This means, inputs can either be chosen at run time (standard), bulk processing support (processing campaign) is available, or triggering services automatically upon occurrence of a specific event (event driven). In order to ensure platform interoperability, openEO functionalities are added to the platform.

Cloud computing capabilities together with availability of datasets makes FS-X suitable for algorithm integration. For algorithm development, prototyping, testing or integration the platform offers application services (e.g. QGIS, SNAP) as well as Jupyter Hub in a basic and data science environment. Algorithms can also be shared with users in the form of services. The following figures show examples of the integration of ARIES results on the platform.

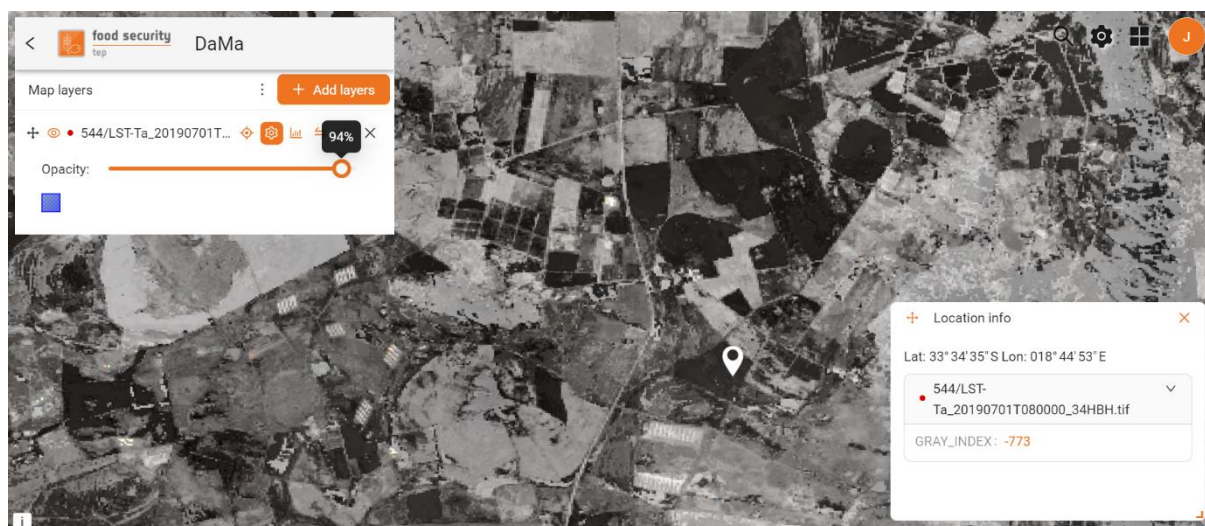


Figure 15: Crop water stress indicator uploaded to the Food Security Explorer platform.

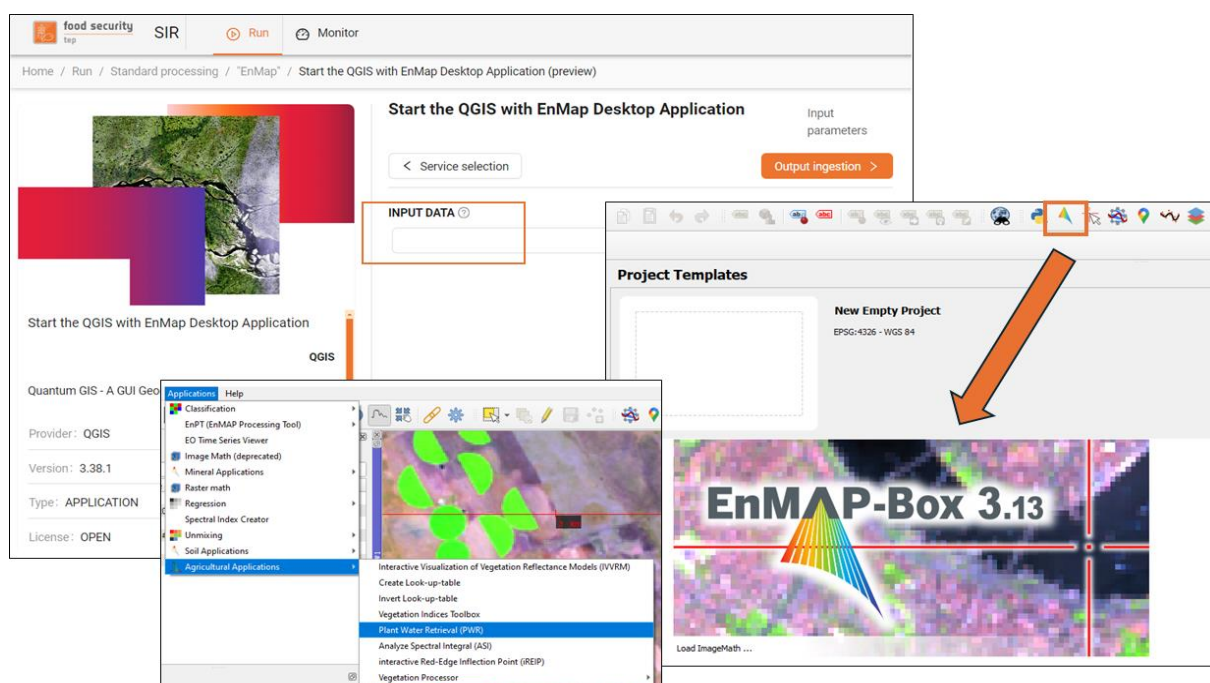
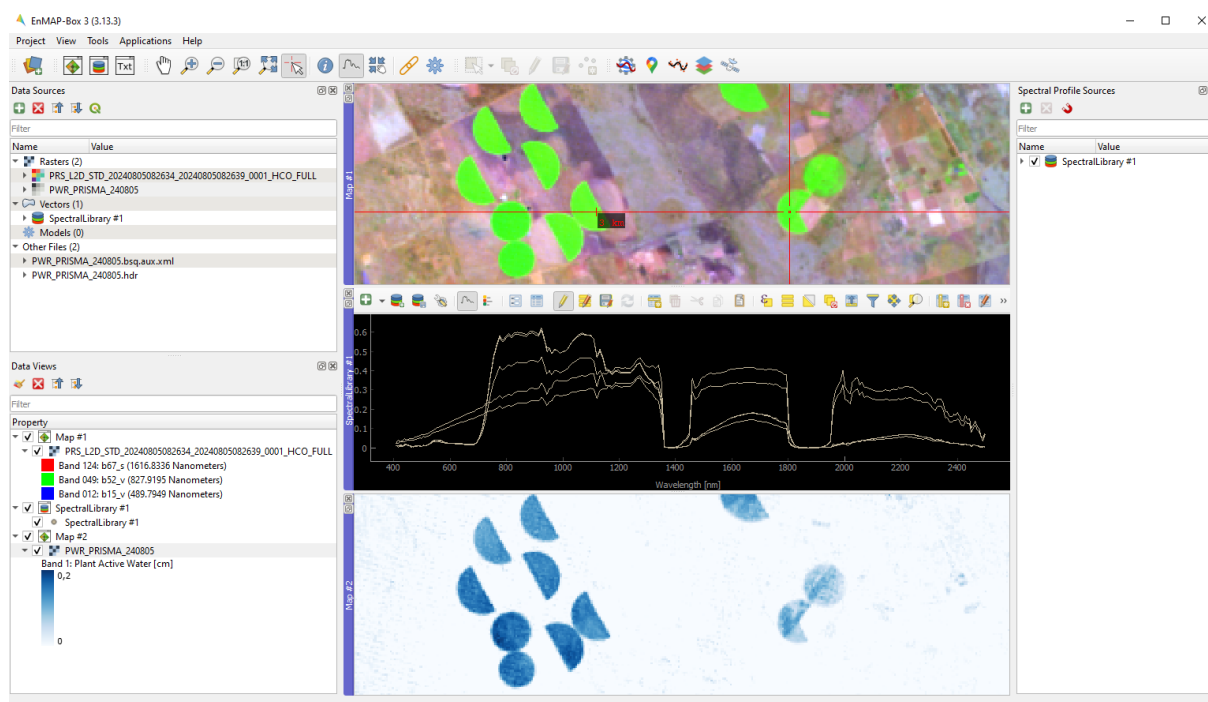


Figure 16: QGIS and EnMAP Toolbox on FS-X. Access to Plant Water Retrieval calculations as example.



**Figure 17: Retrieval of the Plant Water Content using the PWR Algorithm of the EnMAP Toolbox, visualisation as map and spectra of test pixel as illustrated**

## 4 Policy Highlights

Early in the project, a Policy Traceability Matrix has been constructed, summarizing the major policies in place related to natural disasters (and particularly drought) at international, continental and country scale for the three target countries in the project (Zambia, Niger and Kenya). This document already highlighted the added value of climate-smart agriculture and the need for more fine-grained monitoring capabilities in this respect. At the end of the project, we compiled the Policy Highlights document, summarizing the potential impact of the developed indicators (and our enhanced EO-based monitoring capabilities provided by the upcoming satellite missions in general) in light of recent agricultural policy frameworks. The analysis has been restricted to Zambia and the Sahelian region (represented by Niger), two distinctively different use cases in terms of agricultural practices and environmental challenges.

Even though characterized by different agro-climatic, geographical and environmental conditions, the agricultural sectors in both Zambia and the Sahel region face similar challenges, i.e. low agricultural productivity, lack of irrigated agriculture, conflicts on land use and water resources and adverse impacts of climate change. We highlighted various ways in which EO data can support in monitoring and enhancing the effectiveness of agricultural policies, fostering long-term food security and sustainable



land management. Reliable, objective and detailed information on crop types, production, phenology, water stress and health can directly feed into improved land use maps, drought early warning systems, crop water productivity services, agro-pastoralist guidance systems, insurance schemes, seed/input dispersal strategies, climate change mitigation projects and agricultural mechanization policies. Despite this large potential, the adoption of EO data is currently limited in both regions. Capacity development and knowledge transfer therefore remain crucial in boosting the uptake of EO data in the agricultural sector across the continent.

The developed indicators in the framework of the ARIES project are predominantly expected to contribute to improved drought early warning systems and enhancing crop water productivity through improved irrigation advise at field scale.

Future operational missions like CHIME and LSTM will be offering even more detailed measurements of crop health, water usage, and soil conditions. By integrating EO data into policy-making and enforcement, Zambia and Niger can ensure that their agricultural sectors grow sustainably and remain resilient in the face of climate challenges.

## 5 Recommendations for CHIME and LSTM

---

### 5.1 LSTM

- There is a pressing need for a reliable cloud mask. Our analysis revealed significant differences in Land Surface Temperature (LST) between ECOSTRESS and thermally sharpened S3 LST, primarily due to clouds that were not correctly identified by the S3 cloud mask. This discrepancy underscores the importance of enhancing cloud detection capabilities to ensure accurate and consistent LST estimations. Next to that, sufficient research should be devoted towards efficiently filling the observed data gaps, through combination with other data sources such as optical or radar data.
- Safeguarding the accuracy of LST estimation is crucial. S3 data has shown a tendency to overestimate LST, attributed to inaccuracies in assigning land cover types and their corresponding split-window coefficients within the LST retrieval algorithm. Addressing these issues is paramount to rectify biases and enhance the overall reliability of LST data derived from LSTM.
- Implementing a directional correction on the LSTM-derived LST measurements is highly recommended. This correction would not only improve the quality of the LST product by itself, but also enhance comparability with other sensors such as SBG and TRISHNA, hence resulting in a more reliable and consistent daily time series of LST at global scale. A generic directional correction approach, involving one parameter per tile, could already yield notable

improvements. However, for enhanced data consistency, a more refined pixel- or field-specific correction method would be even more beneficial. These enhancements would significantly contribute to the overall effectiveness and accuracy of LSTM in analyzing and generating crop water stress index data.

- Additionally, efforts should be directed towards downscaling other crucial driving data, which also significantly influence ET estimation.

## 5.2 CHIME

- **High spectral quality is of essence for absorption band analysis:** Using small band ratios for absorption analysis means that noise in the images can easily make it impossible to derive accurate quantitative results. Below is an example using EnMAP data and the EnMAP Toolbox to derive plant water content. There is a systematic striping noticeable in the results, which cannot be explained other than with systematic sensor calibration issues. Issues like these will make the accurate retrieval of plant parameters much harder and will hinder user uptake of CHIME.

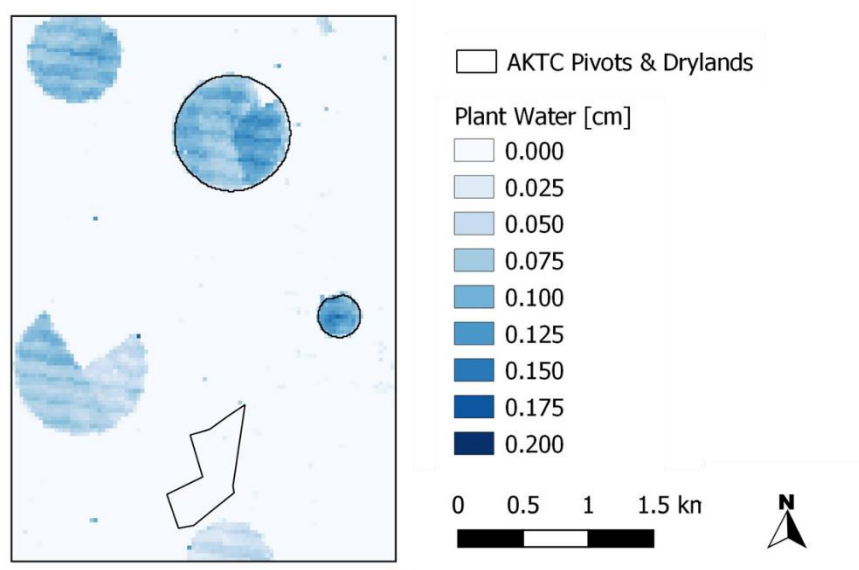


Figure 18: Example of striping in EnMAP data after plant water retrieval with EnMAP toolbox

- **High quality pre-processing:** To fully utilize the information depth of the data, high quality pre-processing is necessary. This obviously includes the spectral domain, but also the spatial domain. A geometric correction that aligns CHIME with Sentinel-2 will make a synergistic use of the two data sources much easier, especially if a (semi-) automated way of time series analysis is the goal. With the current hyperspectral sensors PRISMA and EnMAP, every scene has to be

checked and its location corrected if necessary. This is an extra step, that costs a lot of time and makes the use of available tools that use the field boundaries to mask the image and only produce results for the relevant fields impossible for users who don't have the necessary knowledge on how to geometrically correct the images.

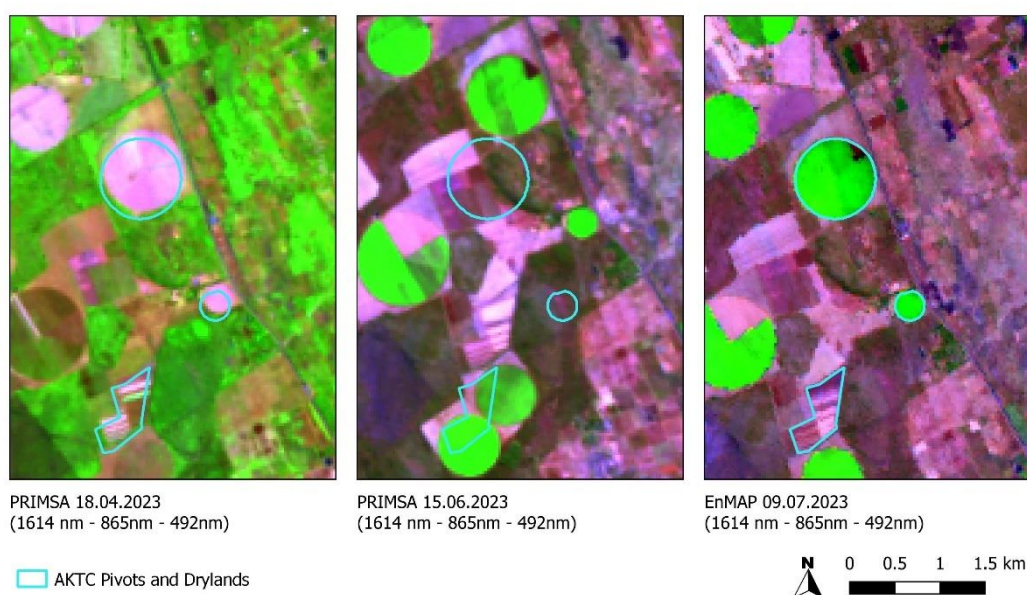


Figure 19: Geometric offsets observed in PRISMA and EnMAP data at the AKTC test site.

- **Tools that can handle the data volume:** Efficient tools that can handle the high dimensionality and large volume of the hyperspectral data without crashing or needing so much time for computation that the delay in agricultural product delivery becomes too long are necessary. Additionally, these tools should be able to process significant areas without loss of efficiency or accuracy, so that the full benefits of the hyperspectral data can be utilized. Parallelized software and cloud computing can support these goals.

## 6 Outreach and Promotion

In the framework of the EOAfrica Explorers ARIES project, two public webinars were organized which served to communicate the project's progress and main outcomes to the African and European EO research communities and potential end users. The first webinar mainly served as a way to closely align the project's scope with the monitoring needs of our Early Adopters. Through a series of presentations and following

discussion, the consortium was able to clarify what could be expected in terms of indicator definition and availability. It also became clear that the potential end users exhibit a high variety in prior skills and expertise when it comes to dealing with and generating geospatial indicators based on EO data. Most of the Early Adopters do not have the means or knowledge to generate the indicators themselves but would rely on technical partners to conduct indicator generation. This has been a valuable lesson for the consortium, as it clearly indicates that future capacity building activities should primarily focus on indicator interpretation, rather than indicator generation. The second webinar was held near the end of the project and focused on the key scientific achievements related to indicator development based on hyperspectral and thermal data, as well as highlighted the integration of our products and workflows in the Food Security Explorer platform.

Additionally, the team participated in several scientific conferences (e.g. ESA's 'International Workshop on High-Resolution Thermal EO', 10-12 May 2023, EO for Agriculture under Pressure 2024 Workshop 13-16 May 2024, EO for Africa Symposium 23 – 26 September 2024) and organized a very successful user workshop at AKTC in Zambia on Sep 12<sup>th</sup> 2024.

## 7 Conclusion

---

The ARIES project successfully developed, validated and prototyped experimental EO analysis techniques for thermal and hyperspectral data to deliver products to improve the monitoring of drought conditions and the detection of crop water stress in support of food security.

Users in Senegal, Mali, Niger, Kenya and Zambia were involved in the project, giving their requirements and giving feedback on the developed products. Interest among the African communities was high, as evidenced by the many and high-ranking participants of the user workshop in Zambia.

One of the main challenges for the validation of the project results was the relatively sparse availability especially of quantitative in-situ validation data. We have thus in some cases resorted to external validation data (e.g. Soil Moisture Data from the International Soil Moisture Network, LAI data calculated from Sentinel-2 multispectral data). In other cases, our methods were chosen to include approaches that have been validated before (e.g. thermal sharpening and plant water retrieval). Also, expert interviews with the African users were conducted. The users could explain the patterns seen in the results and thus validate them.

Based on the Policy Highlights document and discussions with the Early Adopters, it is clear that Earth Observation has a major role to play in monitoring and improving food security in Africa. The new hyperspectral and thermal missions are expected to drastically increase our ability to provide meaningful information in this respect. Based on our experiments, we were able to formulate specific recommendations for further improving these crucial, future missions.

## 8 References

---

### Bibliography Thermal

- AghaKouchak, A., Farahmand, A., Melton, F.S., Teixeira, J., Anderson, M.C., Wardlow, B.D., Hain, C.R., 2015. Remote sensing of drought: Progress, challenges and opportunities. *Reviews of Geophysics* 53, 452–480.
- Bellvert, J., Jofre-Cekalovic, C., Pelechá, A., Mata, M. and Nieto, H. (2020). Feasibility of Using the Two-Source Energy Balance Model (TSEB) with Sentinel-2 and Sentinel-3 Images to Analyze the Spatio-Temporal Variability of Vine Water Status in a Vineyard. *Remote Sensing*, 12, 2299, <https://doi.org/0.3390/rs12142299>
- Fisher, J.B., Lee, B., Purdy, A.J., Halverson, G.H., Dohlen, M.B., Cawse-Nicholson, K., Wang, A., Anderson, R.G., Aragon, B., Arain, M.A., 2020. ECOSTRESS: NASA's next generation mission to measure evapotranspiration from the international space station. *Water Resour Res* 56, e2019WR026058.
- Hadebe, S.T., Modi, A.T., Mabhaudhi, T., 2017. Drought tolerance and water use of cereal crops: A focus on sorghum as a food security crop in sub-Saharan Africa. *J Agron Crop Sci* 203, 177–191.
- Idso, S.B.; Jackson, R.D.; Reginato, R.J. (1977). Remote-Sensing of Crop Yields. *Science*, 196, 19–25.
- Jia, A., Hu, T., Mallick; Kanishka, 2024. Understanding the Sensitivity of Different Drought Indices to Soil Moisture Variations in Africa, in: 104th AMS Annual Meeting. AMS, Baltimore.
- Jia, A., Liang, S., Wang, D., 2022. Generating a 2-km, all-sky, hourly land surface temperature product from Advanced Baseline Imager data. *Remote Sens Environ* 278. <https://doi.org/10.1016/j.rse.2022.113105>
- Lagouarde, J. P., & Irvine, M. (2008). Directional anisotropy in thermal infrared measurements over Toulouse city centre during the CAPITOUL measurement campaigns: First results. *Meteorology and Atmospheric Physics*, 102, 173–185. <https://doi.org/10.1007/S00703-008-0325-4/METRICS>
- Otekunrin, Olutosin Ademola, Otekunrin, Oluwaseun Aramide, Sawicka, B., Ayinde, I.A., 2020. Three decades of fighting against hunger in Africa: Progress, challenges and opportunities. *World Nutrition* 11, 86–111. <https://doi.org/10.26596/wn.202011386-111>
- Pérez-Planells, L., Niclòs, R., Puchades, J., Coll, C., Götsche, F. M., Valiente, J. A., Valor, E., & Galve, J. M. (2021). Validation of sentinel-3 slstr land surface temperature retrieved by the operational product and comparison with explicitly emissivity-dependent algorithms. *Remote Sensing*, 13(11). <https://doi.org/10.3390/rs13112228>
- Sanchez, J. M., Galve, J. M., Nieto, H., & Guzinski, R. (2024). Assessment of High-Resolution LST Derived from the Synergy of Sentinel-2 and Sentinel-3 in Agricultural Areas. *IEEE Journal of Selected Topics in Applied Earth Observations and Remote Sensing*, 17, 916–928. <https://doi.org/10.1109/JSTARS.2023.3335896>

### Bibliography Hyperspectral



- Asner, G. P., Braswell, B. H., Schimel, D. S., & Wessman, C. A. (1998). Ecological research needs from multiangle remote sensing data. *Remote Sensing of Environment*, 63(2), 155–165. [https://doi.org/10.1016/S0034-4257\(97\)00139-9](https://doi.org/10.1016/S0034-4257(97)00139-9)
- Ballaré C.L., Mazza C.A., Austin A.T., Pierik R. (2012) Canopy light and plant health. *Plant Physiology*, 160(1), 145-155. <https://doi.org/10.1104/pp.112.200733>
- Baret, F. (2015). Canopy biophysical variables retrieval from the inversion of reflectance models. In P. S. Thenkabail (Ed.) *Land resources monitoring, modeling, and mapping with remote sensing* (1st ed., Vol. 2, 23–46). Boca Raton, FL: CRC Press
- Berger, K., Atzberger, C., Danner, M., D'Urso, G., Mauser, W., Vuolo, F., & Hank, T. (2018). Evaluation of the PROSAIL model capabilities for future hyperspectral model environments: A review study. *Remote Sensing*, 10(1), 85. <https://doi.org/10.3390/rs10010085>
- Bréda, N. J. J. (2003). Ground-based measurements of leaf area index: A review of methods, instruments and current controversies. *Journal of Experimental Botany*, 54, 2403–2417. <https://doi.org/10.1093/jxb/erg263>
- Chen, J. M. (2018). Remote sensing of leaf area index and clumping index. In Liang, S. (Ed.) *Comprehensive remote sensing*, 53–77. Oxford: Elsevier.
- Fang, H., Baret, F., Plummer, S., & Schaepman-Strub, G. (2019). An overview of global leaf area index (LAI): Methods, products, validation, and applications. *Reviews of Geophysics*, 57, 739–799. <https://doi.org/10.1029/2018RG000608>
- Féret, J. B., François, C., Asner, G. P., Gitelson, A. A., Martin, R. E., Bidet, L. P., Ustin, S.L., Le Maire, G. & Jacquemoud, S. (2008). PROSPECT-4 and 5: Advances in the leaf optical properties model separating photosynthetic pigments. *Remote sensing of environment*, 112(6), 3030-3043. <https://doi.org/10.1016/j.rse.2008.02.012>
- Féret, J. B., Gitelson, A. A., Noble, S. D., & Jacquemoud, S. (2017). PROSPECT-D: Towards modeling leaf optical properties through a complete lifecycle. *Remote Sensing of Environment*, 193, 204-215. <https://doi.org/10.1016/j.rse.2017.03.004>
- Féret J.B., Berger K., de Boissieu F. & Malenovsky Z. 2021. PROSPECT-PRO for estimating content of nitrogen-containing leaf proteins and other carbon-based constituents. *Remote Sensing of Environment*, 252: 112173. <https://doi.org/10.1016/j.rse.2020.112173>
- Fourty, T., Baret, F., Jacquemoud, S., Schmuck, G., & Verdebout, J. (1996). Optical properties of dry plant leaves with explicit description of their biochemical composition: Direct and inverse problems. *Remote Sensing of Environment*, 56, 104–117. [https://doi.org/10.1016/0034-4257\(95\)00234-0](https://doi.org/10.1016/0034-4257(95)00234-0)
- GCOS (2011). Systematic observation requirements for satellite-based products for climate, 2011 Update, Supplemental Details to the Satellite-Based Component of the Implementation Plan for the Global Observing System for Climate in Support of the UNFCCC (2011 Update). Retrieved from <https://climate.esa.int/sites/default/files/gcos-154.pdf>
- Goel, N. S. (1989). Inversion of canopy reflectance models for estimation of biophysical parameters from reflectance data. In Asrar G. (Ed.), *Theory and Applications of Optical Remote Sensing*, 205–251. New York: John Wiley & Sons.
- Goel, N. S., & Thompson, R. L. (2000). A snapshot of canopy reflectance models and a universal model for the radiation regime. *Remote Sensing Reviews*, 18, 197–225. <https://doi.org/10.1080/02757250009532390>
- Houborg, R., Soegaard, H., & Boegh, E. (2007). Combining vegetation index and model inversion methods for the extraction of key vegetation biophysical parameters using Terra and Aqua MODIS reflectance data. *Remote Sensing of Environment*, 106(1), 39–58. <https://doi.org/10.1016/j.rse.2006.07.016>

- Huang, D., Knyazikhin, Y., Wang, W., Deering, D. W., Stenberg, P., Shabanov, N., Tan, B. & Myneni, R.B. (2008). Stochastic transport theory for investigating the three-dimensional canopy structure from space measurements. *Remote Sensing of Environment*, 112(1), 35–50. <https://doi.org/10.1016/j.rse.2006.05.026>
- Jacquemoud, S., Ustin, S. L., Verdebout, J., Schmuck, G., Andreoli, G., & Hosgood, B. (1996). Estimating leaf biochemistry using the PROSPECT leaf optical properties model. *Remote Sensing of Environment*, 56, 194–202. [https://doi.org/10.1016/0034-4257\(95\)00238-3](https://doi.org/10.1016/0034-4257(95)00238-3)
- Jacquemoud, S., Verhoef, W., Baret, F., Bacour, C., Zarco-Tejada, P. J., Asner, G. P., François, C. & Ustin, S. L. (2009). PROSPECT+ SAIL models: A review of use for vegetation characterization. *Remote sensing of environment*, 113, 56 - 66. <https://doi.org/10.1016/j.rse.2008.01.026>.
- Jacquemoud, S., & Baret, F. (1990). PROSPECT: A model of leaf optical properties spectra. *Remote sensing of environment*, 34 (2), 75 – 91. [https://doi.org/10.1016/0034-4257\(90\)90100-Z](https://doi.org/10.1016/0034-4257(90)90100-Z).
- Kuusk, A. (1991). The hot spot effect in plant canopy reflectance. In Myneni, R. B. & Ross, J. (Eds.), *Photon-vegetation interactions. Applications in optical remote sensing and plant ecology*, 139–159. Berlin: Springer Verlag.
- Liang, S. (2004). Quantitative remote sensing of land surfaces. New York: John Wiley and Sons, Inc.
- Le Maire, G. & Francois, C. & Dufrêne, E. (2004). Towards universal broad leaf chlorophyll indices using PROSPECT simulated database and hyperspectral reflectance measurements. *Remote Sensing of Environment*. 89. 1-28. <https://doi.org/10.1016/j.rse.2003.09.004>
- Quemada, C., Pérez-Escudero, J.M., Gonzalo, R., Ederra, I., Santesteban, L.G., Torres, N. & Iriarte J.C. (2021) Remote Sensing for Plant Water Content Monitoring: A Review. *Remote Sensing*. 13(11):2088. <https://doi.org/10.3390/rs13112088>
- Running, S.W., Gower, S. (1991). Forest-BGC, a general model of forest ecosystem processes for regional applications. II. Dynamic carbon allocation and nitrogen budgets. *Tree Physiology*, 9, 147–160. [https://doi.org/10.1016/0304-3800\(88\)90112-3](https://doi.org/10.1016/0304-3800(88)90112-3)
- Tagliabue, G., Boschetti, M., Bramati, G., Candiani, G., Colombo, R., Nutini, F., Pompilio, L., Rivera-Caicedo, J. P., Rossi, M., Rossini, M., Verrelst, J., & Panigada, C. (2022). Hybrid retrieval of crop traits from multi-temporal PRISMA hyperspectral imagery. *ISPRS Journal of Photogrammetry and Remote Sensing*, 187, 362–377. <https://doi.org/10.1016/j.isprsjprs.2022.03.014>
- Verhoef, W. (1984). Light scattering by leaf layers with application to canopy reflectance modeling: the SAIL model. *Remote Sensing of Environment*, 16, 125–141. [https://doi.org/10.1016/0034-4257\(84\)90057-9](https://doi.org/10.1016/0034-4257(84)90057-9)
- Verhoef, W. & Bach, H. (2003). Simulation of hyperspectral and directional radiance images using coupled biophysical and atmospheric radiative transfer models. *Remote Sensing of Environment*, 87, 23–41. [https://doi.org/10.1016/S0034-4257\(03\)00143-3](https://doi.org/10.1016/S0034-4257(03)00143-3)
- Verhoef, W., & Bach, H. (2007). Coupled soil-leaf-canopy and atmosphere radiative transfer modeling to simulate hyperspectral multi-angular surface reflectance and TOA radiance data. *Remote Sensing of Environment*, 109, 166–182. <https://doi.org/10.1016/j.rse.2006.12.013>
- Verhoef, W., Xiao, Q., Jia, L., & Su, Z. (2007). Unified optical-thermal four-stream radiative transfer theory for homogeneous vegetation canopies. *IEEE Transactions on Geoscience and Remote Sensing*, 45, 1808–1822. <https://doi.org/10.1109/TGRS.2007.895844>
- Verrelst, J., Rivera, J. P., Leonenko, G., Alonso, L., & Moreno, J. (2014). Optimizing LUT-based RTM inversion for semiautomatic mapping of crop biophysical parameters from Sentinel-2 and -3 data: Role of cost functions. *IEEE Transactions on Geoscience and Remote Sensing*, 52(1), 257–269. <https://doi.org/10.1109/TGRS.2013.2238242>
- Verrelst, J., Rivera, J. P., Veroustraete, F., Muñoz-Marí, J., Clevers, J. G. P. W., Camps-Valls, G., & Moreno, J. (2015). Experimental Sentinel-2 LAI estimation using parametric, non-parametric and

physical retrieval methods—A comparison. *ISPRS Journal of Photogrammetry and Remote Sensing*, 108, 260–272. <https://doi.org/10.1016/j.isprsjprs.2015.04.013>

Watson, D.J. (1947). Comparative physiological studies on the growth of field crops: I. Variation in net assimilation rate and leaf area between species and varieties and within and between years. *Annals of Botany*. 11: 41–76. <https://doi.org/10.1093/oxfordjournals.aob.a083148>.

Weiss, M., Troufleau, D., Baret, F., Chauki, H., Prévot, L., Olivoso, A., Bruguier, N. & Brisson, N. (2001). Coupling canopy functioning and radiative transfer models for remote sensing data assimilation. *Agricultural and Forest Meteorology*, 108, 113–128. [https://doi.org/10.1016/S0168-1923\(01\)00234-9](https://doi.org/10.1016/S0168-1923(01)00234-9)

Woher, M., Berger, K., Danner, M., Mauser, W., & Hank, T. (2018). Physically-Based Retrieval of Canopy Equivalent Water Thickness Using Hyperspectral Data. *Remote Sensing*, 10, 1924. <https://doi.org/10.3390/rs10121924>

Zheng, G., & Moskal, L. M. (2009). Retrieving leaf area index (LAI) using remote sensing: Theories, methods and sensors. *Sensors*, 9(4), 2719–2745. <https://doi.org/10.3390/s90402719>